

***In-vivo* high resolution AFM topographic imaging of
Caenorhabditis elegans reveals previously unreported surface
structures of cuticle mutants**

Clara L Essmann^{1*}, PhD; Muna Elmi¹, PhD; Mike Shaw^{1,2}, PhD; Giridhar M
Anand^{1,3}; Vijay M. Pawar, PhD¹; Mandayam A Srinivasan, Prof.^{1,4}

¹ - UCL TouchLab, Department of Computer Science, University College London,
Engineering Building, Malet Place, London, WC1E 7JG, UK

² Analytical Science Division, National Physical Laboratory, Teddington,
Middlesex, TW11 0LW, UK

³ Massachusetts Institute of Technology, Cambridge, MA 02139, USA

⁴ MIT Touchlab, Department of Mechanical Engineering and Research Laboratory
of Electronics, Massachusetts Institute of Technology, Cambridge, MA 02139,
USA

* corresponding author. Department of Computer Science, University College
London, Engineering Building, Malet Place, London, WC1E7JG, UK

Phone: 0044(0)20 7679 3698 email: c.essmann@ucl.ac.uk

CONFLICT OF INTEREST

The authors declare that there are no conflicts of interest.

FUNDING

This work is part funded by the European Research Council Advanced Grant: 247041 (MicroNanoTeleHaptics) and the Engineering and Physical Sciences Research Council Grant: EP/K005030/1 (Robotic Teleoperation for Multiple Scales: Enabling Exploration, Manipulation and Assembly Tasks in New Worlds).

Word count for abstract: 150

Word count for manuscript: 1497

Number of references: 25

Number of figures: 5

Number of tables: 0

Number of supplementary online-only files: 3

Abstract

Atomic force microscopy (AFM) is a powerful method for topographic imaging of surfaces with nanometer resolution. AFM offers significant advantages over scanning electron microscopy (SEM) including the acquisition of quantitative 3D-images and biomechanical information. More importantly, for in-vivo biological imaging, AFM does not require sample dehydration/labeling. We show for the first time high-resolution topographical images of the cuticle of the model organism *C. elegans* under physiological conditions using AFM. *C. elegans* is used extensively for drug screening and to study pathogen adherence in innate immunity; both applications highly depend on the integrity of the nematode's cuticle. Mutations affecting both drug adsorption and pathogen clearance have been proposed to relate to changes in the cuticle structure, but never visually examined in high resolution. In this study we use AFM to visualize the topography of wild-type adult *C. elegans* as well as several cuticle collagen mutants and describe previously unseen anatomical differences.

Keywords

Atomic force microscopy, nano-scale topography, *C. elegans*, cuticle mutants, collagens

Background

AFM achieves nanometer level resolution under ambient conditions, offering exciting possibilities for imaging biological samples [1–3]. Although SEM can achieve similar resolution, it requires fixative treatment of the sample including harsh dehydration steps [4]. In this study we characterize the topographical and biomechanical properties of the cuticle of the model organism *C. elegans*. *C. elegans* is used in medical research for high-throughput drug screening and pathogen host interaction studies, and its cuticle is layered similarly to human skin [5–8]. Both research applications are critically dependent on the animal's cuticle, and mutations in cuticle proteins can influence both efficiency of drug uptake and resistance to pathogens or biofilm formation [9–11]. Several SEM studies have described the gross surface structure of the cuticle, while TEM sections reveal the structure of the cuticle sub-layers [8,12,13]. A published AFM study was limited to fixed, partially dry larval stage animals [14]. Therefore, the nano-scale topography of adult *C. elegans* cuticle under physiological conditions and its biomechanical properties, including the differences between wild-type strains and relevant cuticle mutants, remain undescribed. Our study shows for the first time AFM topography images of live adult wild-type worms and reveals new surface structures in collagen mutants.

Methods

Strains

All strains were cultivated at 20°C and maintained as described previously [15]. N2 (wild-type), CB61 (*dpy-5*), CB88 (*dpy-7*), CB128 (*dpy-10*), CB458 (*dpy-13*)

strains were obtained from the Caenorhabditis Genetics Center (University of Minnesota).

Worm preparation for AFM

Staged young adult worms were paralysed (10mg/ml BDM), fixed on head and tail with tissue glue (Dermabond) onto an agarose pad in a dish and immersed in 2.5ml M9-buffer to prevent dehydration. For SEM-fixation, staged young adults were fixed in 3% glutaraldehyde o/n.

AFM

AFM images of worms were obtained using a NanoWizard3 (JPK). Type qp-CONT-10 (nanosensors) cantilevers were used for imaging in contact-mode and NSC18/no AL (MikroMasch) for quantitative imaging (QI) mode. The setpoint for imaging was 0.3V (~350pN) at 0.5Hz scanning speed and for QI 0.3V (35nN) at 100µm/s. Cantilever sensitivity and spring constant were calibrated using the JPK calibration tool [16].

Optical imaging

Staged young adults were stained with the fluorescent lipophilic dye DiI [17], paralyzed and mounted on a 2% agarose pad in M9 buffer. Focal image series were captured using an upright epifluorescence microscope (BX51WI, Olympus) with a 60x/1.0 objective lens.

Image analysis

AFM data was analysed using JPK analysis software. Topography images are flattened (256x256 pixels) and the elastic modulus was calculated using the Hertz/Sneddon contact mechanics model (image 128x128 pixels). Optical images were processed and analysed using custom scripts written in Matlab and ImageJ.

Results

An AFM was used to obtain topographic images of the cuticle of wild-type *C. elegans* under physiological conditions (methods). The major surface structures include the alae, three parallel ridges along the length of the worm on either side of the body, and a series of periodically separated annuli and furrows running perpendicular to the alae (Figure 1A). Using soft cantilevers, optimized for contact-mode imaging in solution, an area of 10x10 μ m was scanned at the worm surface (Figure 1B). The analyzed image shows the ring-like segments of the worm including annuli and furrows (Figure 1B).

Next we imaged the surface of two different cuticle collagen mutants that are longer (*lon-2*) or shorter (*dpy-5*) than wild-type worms (Figure 2A) and compared their 3D-structure to that of wild-type animals. Quantifications of annuli width and furrow depth show correlations to the body size of the animals and suggest that the total number of annuli is the same for wild-type, *dpy-5* and *lon-2*. Measured annuli depth and width may depend on scanning force applied, but the line profiles did not change at higher scan forces (Figure 2B-F).

Next we analyzed additional mutants, one with annuli (*dpy-13*) and two in which the cuticle has been reported to lack annuli and furrows (*dpy-7*, *dpy-10*) [13]. *Dpy-13* animals show similar size/annuli ratios as *dpy-5* and wild-type animals, confirming a common total number of annuli for each organism (Figure 3B). Surprisingly, and in contrast to their smooth appearance in SEM images, AFM images of mutants without annuli reveal irregular surface patterns of similar height and depth as *dpy-5* animals (Figure 3A).

We confirmed our AFM surface analysis results by performing fluorescence imaging of DiI stained animals (Figure 4A). Deconvolved focal series of images were analyzed for annuli width and matched the AFM results (Figure 4B). When viewed as a maximum intensity projection, the cuticles of both non-annuli mutants appeared smooth in the optical images, similar to published SEM results. However, single viewing image planes reveal irregular net-like structures consistent with the AFM results (Figure 4C).

To investigate whether sample preparation for SEM accounts for differences in the appearance of the cuticle, non-annuli mutants were treated with 3% glutaraldehyde, a fixative used for SEM [13,18]. Comparing AFM images of fixed and non-fixed mutants reveals a slight reduction in surface details, however the cuticle still contained significant topographic structures (Figure 5A).

To characterize biomechanical properties of the *C. elegans* cuticle we utilized the QI mode of the AFM, in which force-distance curves are recorded to determine topography and local mechanical properties [19]. We applied the Hertz/Sneddon contact mechanics model for small indentations considering the tip-shape of the indenter to estimate the Elastic Modulus at each location (Figure 5B, Suppl Figure 2), RMS is in Figure 5D [20–22]. A 3D-overlay of topography and Elastic Modulus of the worm cuticle indicates that minimum values occur in annuli regions and maximal values in the furrows, the indentation depth is approximately 500nm (Figure 5C). The overall values are within the range of previously described data for *C. elegans* cuticle [23,24].

Discussion

We developed an experimental protocol to acquire high-resolution 3D surface topography data of paralyzed young adult *C. elegans* using AFM. In contrast to SEM, which requires dehydrated samples held under vacuum, our methodology enabled organisms to be imaged *in-vivo* under physiological conditions. Our results revealed previously unreported surface structures in *C. elegans* cuticle mutants which appeared smooth using SEM. Treating the worms with SEM fixative did not significantly remove the surface structure suggesting that subsequent dehydration steps, gold-particle coating, or data analysis might explain these differences. In particular, ethanol dehydration is likely to affect cuticle proteins, which are ethanol-soluble [25]. *C. elegans* is widely used in clinical research for drug screening and pathogen adherence studies. Mutations in cuticle proteins (e.g. *bus-5*, *srf-3*) affect the integrity of the cuticle and therefore pathogen adherence [10,11] and drug uptake efficiency. In most cases the changes are attributed to the surface topography of these mutants but evidence is limited. Our AFM imaging technique offers an exciting new possibility to visualize and characterize these cuticle mutants. In addition to the acquisition of detailed surface images we were able to measure force-displacement relationship and estimate cuticle elasticity. We have shown that QI imaging allows insights into spatial variations of stiffness (furrows stiffer than annuli) providing more detailed information about the cuticle's biomechanics. One possible explanation is that the collagen layer above the hypodermis and muscles is thinner in furrows, and that furrows are supported by collagen struts

[8]. Moreover, actin bundles at the apical layer of the hypodermis assisting to structure the furrows might contribute to the higher stiffness.

Together with topographic images, local biomechanical properties of cuticle mutants could shed light on the function of the mutated cuticle proteins like collagens, which remain largely unknown.

References

1. Kasas S, Thomson N. Biological applications of the AFM: from single molecules to organs. ... *J. Imaging* 8(2), 151–161 (1997).
2. Goldsbury CS, Scheuring S, Kreplak L. Introduction to atomic force microscopy (AFM) in biology. *Curr. Protoc. Protein Sci.* Chapter 17(November), Unit 17.7.1–19 (2009).
3. Jalili N, Laxminarayana K. A review of atomic force microscopy imaging systems: application to molecular metrology and biological sciences. *Mechatronics*. 14(8), 907–945 (2004).
4. Russell P, Batchelor D, Facility AI, Russell PE. SEM and AFM : Complementary Techniques for Surface Investigations. *Microsc. Anal.* , 9–12 (2001).
5. Kaletta T, Hengartner MO. Finding function in novel targets: *C. elegans* as a model organism. *Nat. Rev. Drug Discov.* 5(5), 387–398 (2006).
6. Markaki M, Tavernarakis N. Modeling human diseases in *Caenorhabditis elegans*. *Biotechnol. J.* 5(12), 1261–1276 (2010).
7. O'Reilly LP, Luke CJ, Perlmutter DH, Silverman G a., Pak SC. *C. elegans* in high-throughput drug discovery. *Adv. Drug Deliv. Rev.* 69-70, 247–253 (2014).
8. Altun ZF, Hall DH. Worm Atlas [Internet]. WORMATLAS. (2009). Available from: <http://www.wormatlas.org/hermaphrodite/seamcells/Seamframeset.html>.
9. Darby C, Chakraborti A, Politz SM, Daniels CC, Tan L, Drace K. *Caenorhabditis elegans* mutants resistant to attachment of *Yersinia* biofilms. *Genetics*. 176(1), 221–230 (2007).
10. Hodgkin J, Kuwabara PE, Corneliussen B. A novel bacterial pathogen, *Microbacterium nematophilum*, induces morphological change in the nematode *C. elegans*. *Curr. Biol.* 10(24), 1615–1618 (2000).

11. Gravato-Nobre MJ, Nicholas HR, Nijland R, *et al.* Multiple genes affect sensitivity of *Caenorhabditis elegans* to the bacterial pathogen *Microbacterium nematophilum*. *Genetics*. 171(3), 1033–1045 (2005).
12. Page AP, Johnstone IL. The cuticle. *WormBook*. , 1–15 (2007).
13. McMahon L, Muriel JM, Roberts B, Quinn M, Johnstone IL. Two sets of interacting collagens form functionally distinct substructures within a *Caenorhabditis elegans* extracellular matrix. *Mol. Biol. Cell*. 14(4), 1366–1378 (2003).
14. Allen MJ, Kanteti R, Riehm JJ, El-Hashani E, Salgia R. Whole-animal mounts of *Caenorhabditis elegans* for 3D imaging using atomic force microscopy. *Nanomedicine*. 11(8), 1971–4 (2015).
15. Brenner S. The genetics of *Caenorhabditis elegans*. *Genetics*. 77(1), 71–94 (1974).
16. JPK. Summary Notes – Force spectroscopy measurements and processing. *JPK instruments Tech. Summ.* (May) (2009).
17. Schultz RD, Gumienny TL. Visualization of *Caenorhabditis Elegans* Cuticle Structures Using the Lipophilic Vital Dye, Dil. *J. Vis. Exp.* (59), 1–6 (2012).
18. Hall DH, Hartweg E, Nguyen KCQ. Modern electron microscopy methods for *C. elegans*. In: *Methods in cell biology*. , 93–149 (2012).
19. Haschke H, Jähnke T. QI offers next-generation AFM imaging mode for nanometrology. *Laser Focus World*. 48(3), 25–30 (2012).
20. Hertz H. Über die Berührung fester elastischer Körper. *J. für die reine und Angew. Math.* 171, 156–171 (1881).
21. Sneddon IN. The relation between load and penetration in the axisymmetric boussinesq problem for a punch of arbitrary profile. *Int. J. Eng. Sci.* 3(1), 47–57 (1965).
22. Lin DC, Dimitriadis EK, Horkay F. Robust strategies for automated AFM force curve analysis--I. Non-adhesive indentation of soft, inhomogeneous materials. *J Biomech Eng.* 129(3), 430–440 (2007).

23. Sznitman J, Purohit PK, Krajacic P, Lamitina T, Arratia PE. Material properties of *Caenorhabditis elegans* swimming at low Reynolds number. *Biophys. J.* 98(4), 617–26 (2010).
24. Backholm M. Viscoelastic properties of the nematode *Caenorhabditis elegans*, a self-similar, shear-thinning worm. *Proc.* 110(12), 4528–33 (2013).
25. Page AP, Rudin W, Fluri E, Blaxter ML, Maizels RM. *Toxocara canis*: a labile antigenic surface coat overlying the epicuticle of infective larvae. *Exp. Parasitol.* 75(1), 72–86 (1992).

Figure legends

Figure 1: Cuticle structures in *C. elegans*. **A** Optical image of wild-type *C. elegans* (top) and schematic diagram showing annuli, furrows and alae (bottom). **B** Optical image from our AFM setup showing the cantilever and body of the worm (top) and typical topography image of the cuticle (bottom).

Figure 2: Analysis of wild-type *C. elegans* and cuticle mutant surface structures. **A** Brightfield images of wild-type and mutants (*dpy-5*, *lon-2*). **B** AFM topography images (top) and line histograms (bottom) of wild-type, *dpy-5* and *lon-2* animals. **C+D** Comparison of annuli/furrow width for wild-type and mutants represented as mean \pm SEM, $n > 30$. **E** Line profiles for topographic images with increasing scan force. **F** Comparison of body size of wild-type and mutants represented as mean \pm SEM, $n > 19$. **G** Comparison of body size and annuli width of mutants represented as percentage of wild-type.

Figure 3: Comparison of mutants with and without annuli. **A** AFM topography images and corresponding line profiles. **B** Measured body size and annuli width of mutants represented as percentage of wild-type.

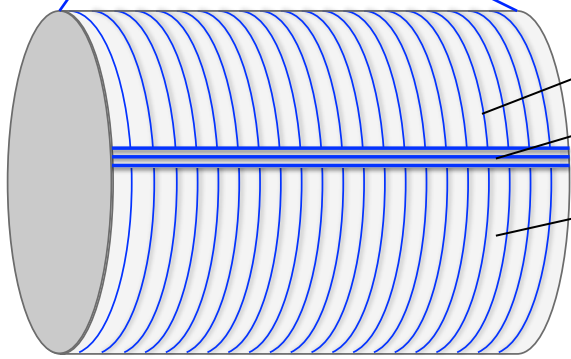
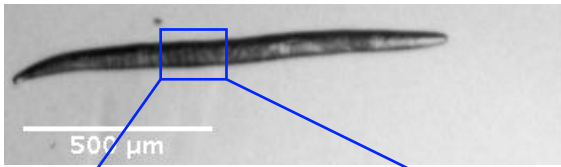
Figure 4: Fluorescence imaging of surface structures. **A** Representative images of deconvolved axial image projections of wild-type and mutants stained with DiI (see methods). Insets showing surface structures (annuli, furrows) highlighted by DiI staining. **B** Comparison of annuli width from AFM and fluorescence images of wild-type and mutants represented as mean \pm SEM, $n > 30$ (AFM), $n > 8$

(Fluorescence). **C** Transverse image section showing DiI-highlighted structures in mutants.

Figure 5: Surface characteristics. **A** AFM topography images of non-annuli mutants without and without SEM-fixative treatment. **B** AFM images of wild-type animals acquired in QI mode: topography (upper panel), Elastic Modulus (lower panel) **C** 3D-overlay of topography and Elastic Modulus from B. **D** RMS histogram shows accuracy of the fit.

Figure 1

A



B

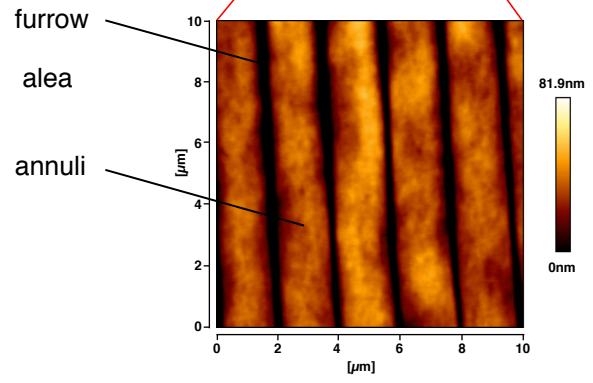
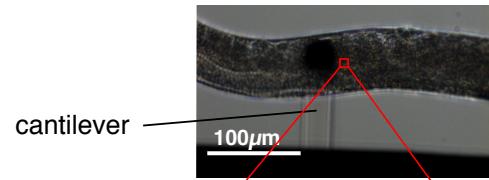
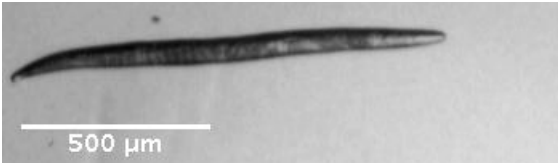


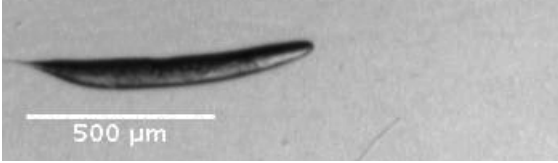
Figure 2

A

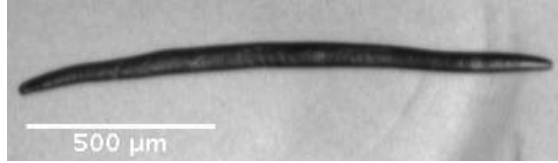
wild-type



dpy-5

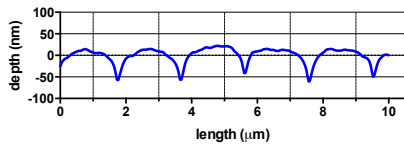
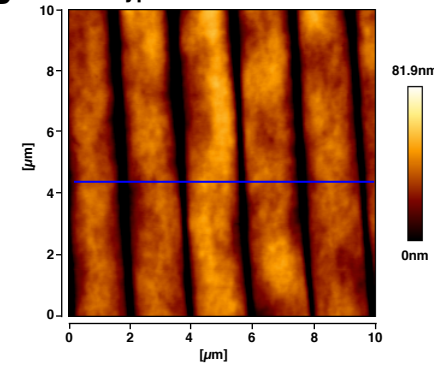


lon-2

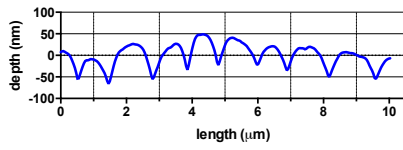
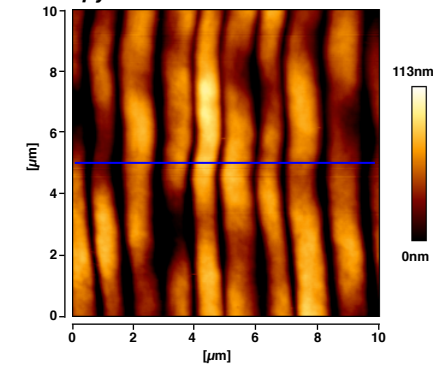


B

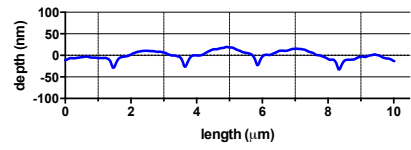
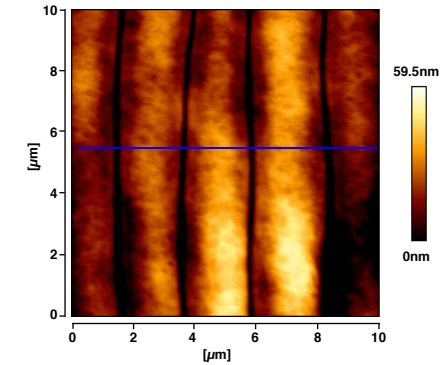
wild-type



dpy-5

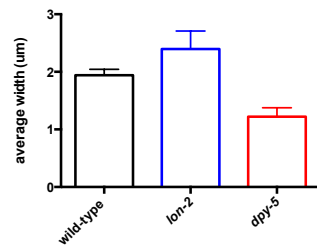


lon-2



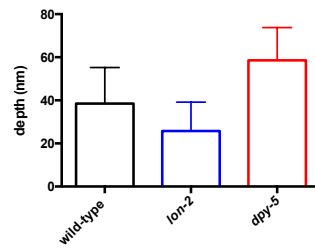
C

annuli width



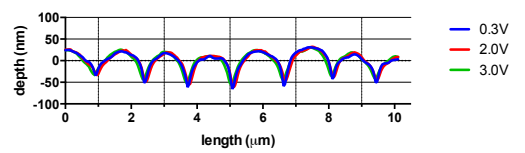
D

furrow depth



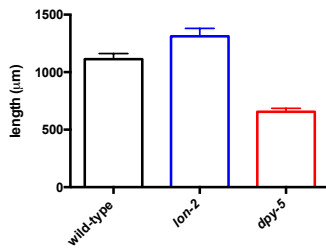
E

line profile with increasing scan force



F

length young adults



G

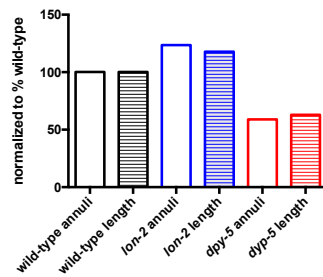
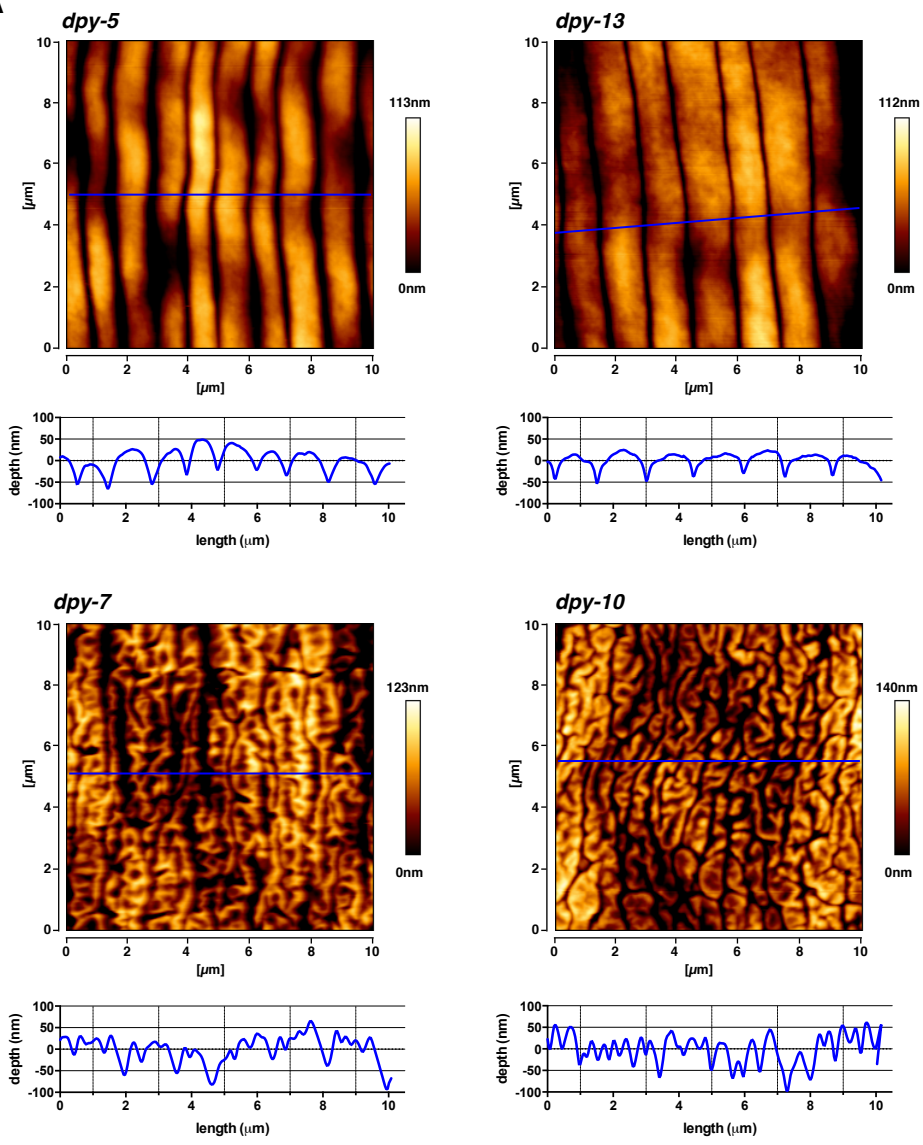


Figure 3

A



B

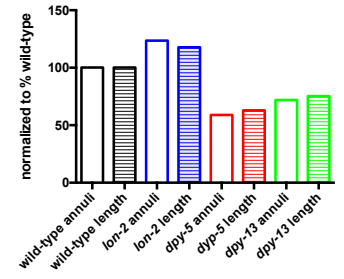
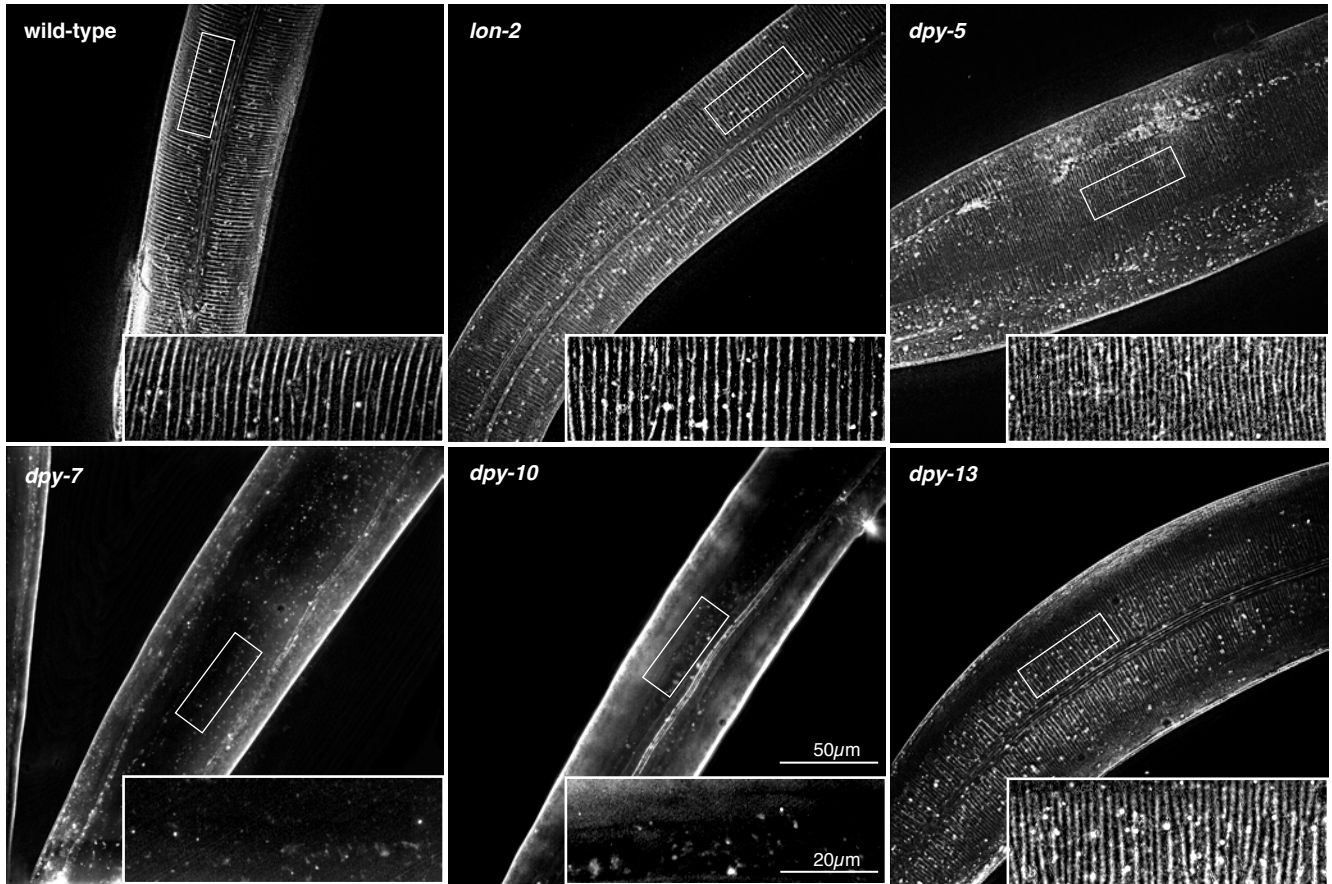
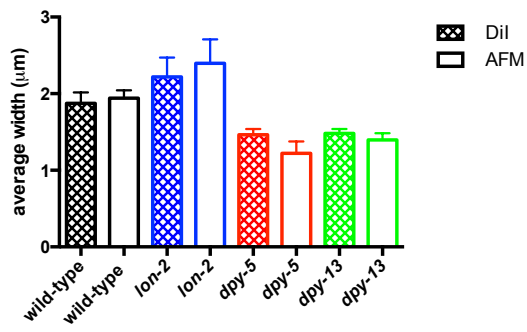


Figure 4

A



B



C

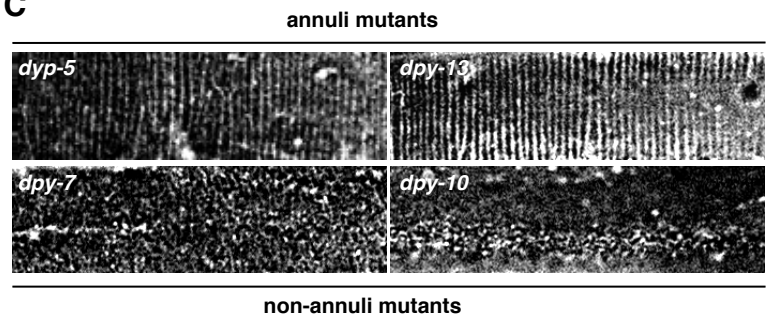
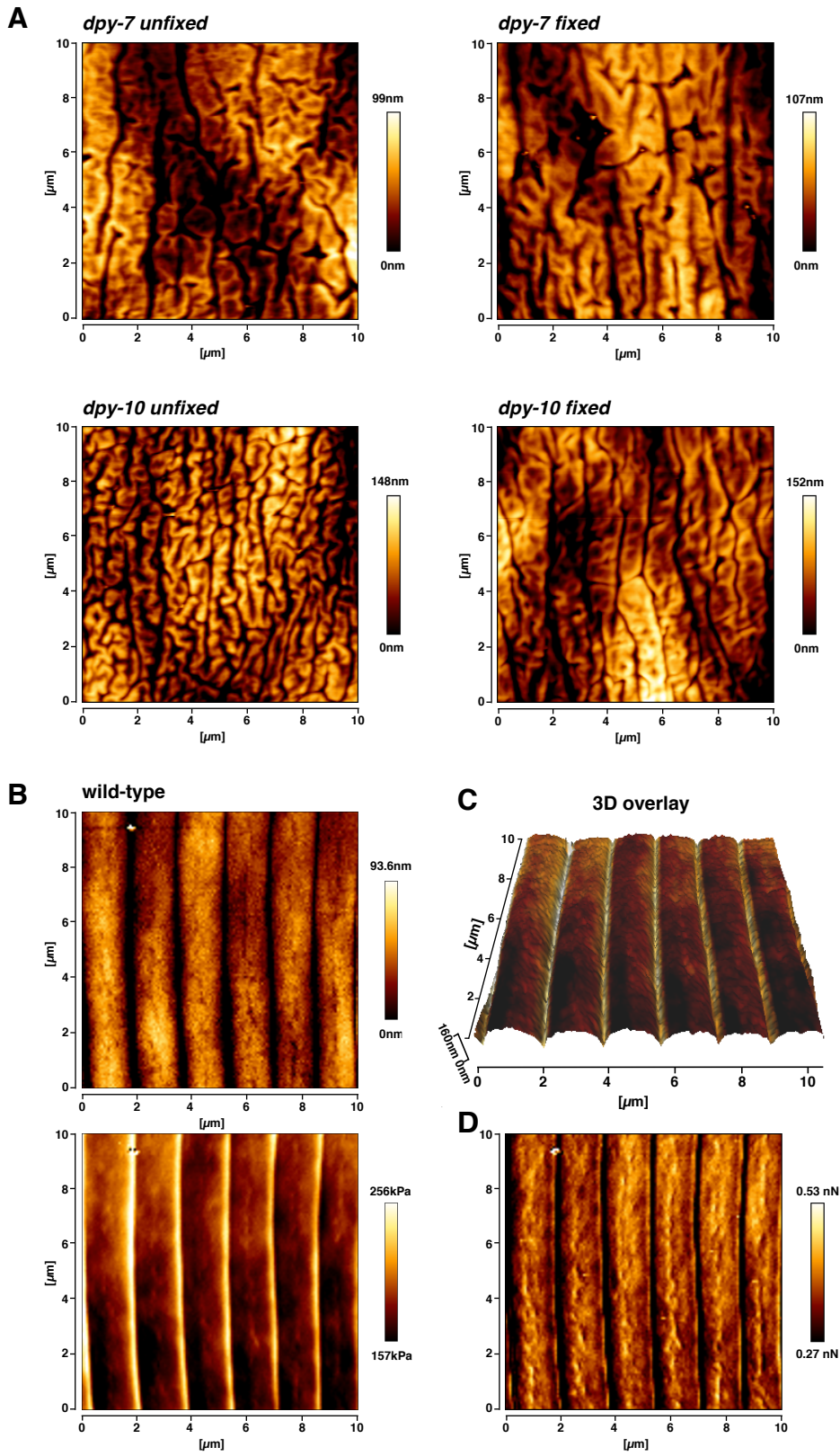
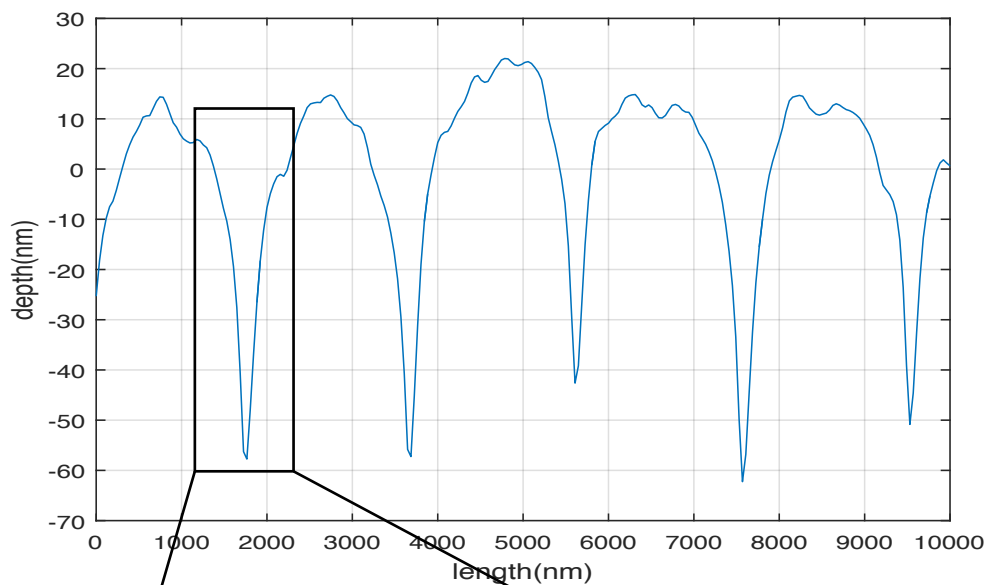


Figure 5

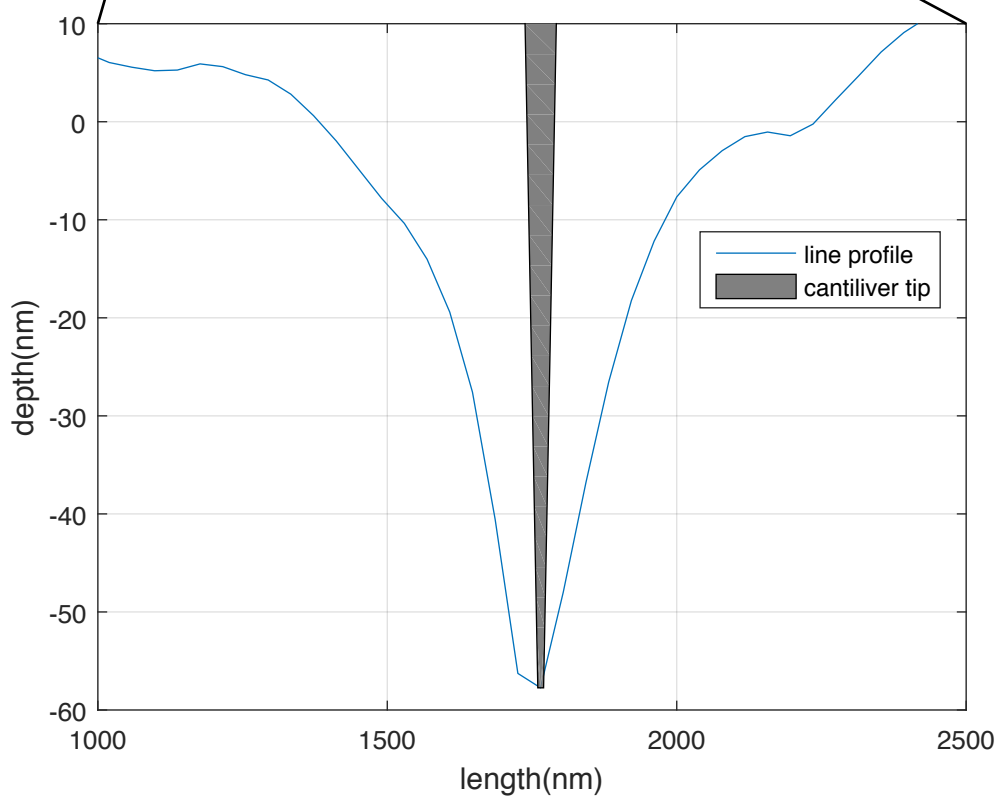


Supplementary Figure 1

A Line histogram from AFM image



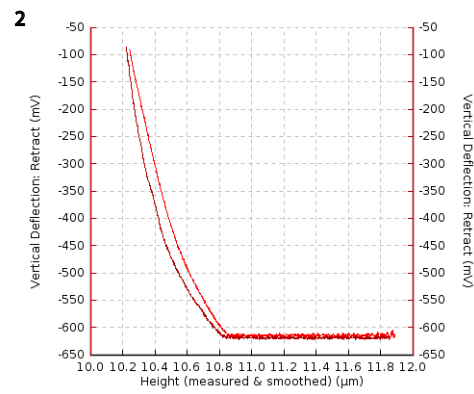
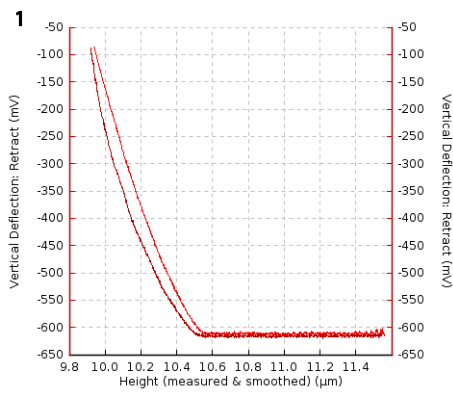
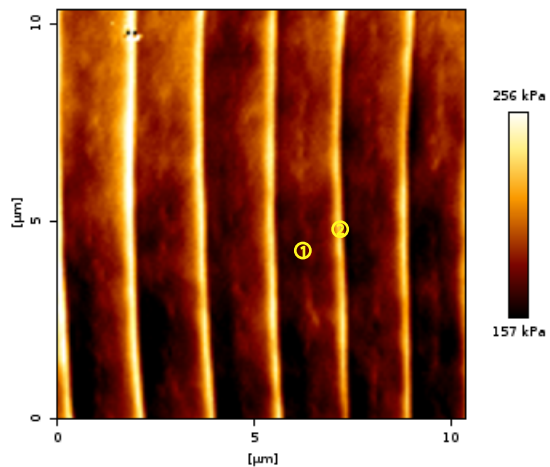
B Dimension between tip and sample



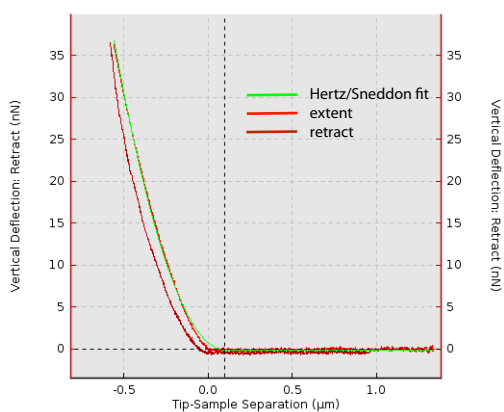
Supplementary Figure 1: Tip-sample size relation. **A** Line histogram of an AFM image shows outline of the surface of a worm (upper panel). A grey box indicates the location of the tip-sample-scale illustration (lower panel). Note the scale difference of x-axis and y-axis. **B** Tip-sample-scale illustration showing size relation of tip versus sample outline. The tip radius is $>10\text{nm}$. Note the scale difference between x-axis and y-axis.

Supplementary Figure 2

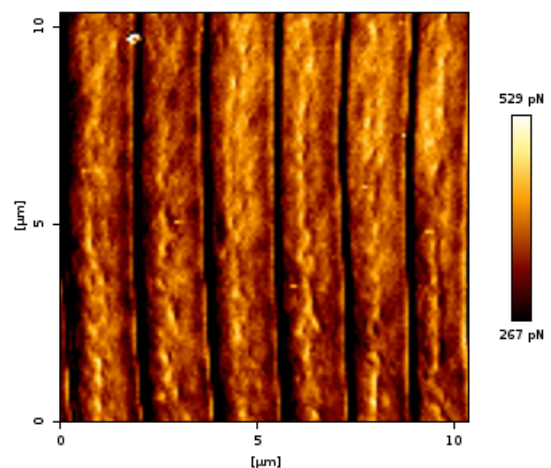
A Elastic Modulus of the cuticle



B Hertz/Sneddon fit on force-distance curve



C Residual RMS of the Hertz/Sneddon fit



Supplementary Figure 2: Estimated Elastic Modulus of the worm cuticle **A** Elastic Modulus of worm cuticle acquired from Hertz/Sneddon fit on QI mode AFM data (128x128 pixels). Furrows appear stiffer than annuli regions (upper panel). Numbers in yellow circles indicate the location of two example V/z curves. **B** Example force-distance curve with Hertz/Sneddon fit (green). **C** Residual RMS indicates the difference between force curve and Hertz/Sneddon fit in pN.